Solvation of Metal Nanoparticles in a Subcritical — Supercritical Fluid: A Computer Simulation Study

Moti Lal,*,† Martin Plummer,‡ Nicola J. Richmond,†,§ and William Smith‡

Centre for Nanoscale Science, The Donnan and Robert Robinson Laboratories, University of Liverpool, Liverpool L69 7ZD, U.K., and Computational Science & Engineering Department, CCLRC Daresbury Laboratory, Daresbury, Cheshire WA4 4AD, U.K.

Received: September 17, 2003; In Final Form: February 13, 2004

Molecular dynamics simulations of passivated and bare gold nanoparticles immersed in ethane have been performed in the reduced temperature ($T_r = T/T_c$) range 0.95−1.05 along the critical isochore of the solvent. The effects of temperature and passivation on the radial distribution of the solvent molecules about the center of mass of the metal core and on the degree of solvation (ϑ) have been investigated. The results show that the solvation of the 38-atom bare particle is *qualitatively* different from that of the passivated particle: the degree of solvation of the bare particle is *positive*, whereas it is *negative* for the passivated particle. This difference in the solvation propensity of the particle in the presence and absence of the passivating layer is attributed to the different forces controlling the solvation process in the two cases. It is found that the degree of solvation of the 8-atom-core passivated particle is greater than that of the 38-atom-core passivated particle, due essentially to different configurational structures assumed by the passivating layers of the smaller and the larger particle. For the bare particle, the degree of solvation as a function of temperature passes through a maximum, a manifestation of the enhancement effect produced in the clustering of the solvent molecules around the solute as the system moves toward the critical point. The initial, minimum-energy configuration of the particle cores underwent appreciable changes as the system approached the equilibrium state in the simulations.

1. Introduction

The phenomenal surge of interest in nano-objects (metal-atom clusters, fullerenes, carbon nanotubes, nanowires, nanotapes, etc.) is due to their extraordinary optical, electronic, magnetic, and conducting properties that differ significantly, and often qualitatively, from those of the corresponding bulk materials.[1] In their properties lies the promise for a technological revolution[1,2] in areas like optoelectronics, magnetic storage, sensing technologies, catalysis, and fuel storage. In addition to the structural and chemical characteristics, factors that feature crucially in the determination of the various properties of nano objects are their size and shape.[3−5] Therefore, a key requirement for pursuing systematic and accurate studies of these objects, with both scientific and technological objectives in mind, is the availability of the samples of narrow-size distribution. Whetten et al.,[6−8] as well as others,[9] succeeded in separating polydisperse samples of passivated metal nanoparticles into various size fractions by progressively adding an antisolvent into the particle dispersion, which resulted in the sequential precipitation of the particles in order of their size, the largest particles precipitating first. Another technique used by the same workers[6] was liquid gravity column chromatography, which allowed them to separate 38-atom gold particles from the polydisperse dispersion.

More recently, supercritical fluids have been investigated for their efficacy as fractionating media for nanoparticles. The experimental results obtained by Clark et al.[10] and subsequently by Shah et al.[11] on the size-selective dispersibility of alkane thioate coated gold nanoparticles in supercritical ethane show significant promise: the former group demonstrated the preferential dispersion of smaller size particles in a bimodal sample, and the latter group established the possibility of tuning the dispersing power of the supercritical medium by density changes. They rationalized the observed behavior in terms of the colloid theory,[12] which combines Hamaker's theory of van der Waals forces with the theory of steric stabilization. Shah et al.[11] thus provided a phenomenological interpretation of the density-dependent dispersing power of the fluid.

With respect to their dimensions, nanoparticles are closer to molecules than to colloids, warranting their treatment in terms of models that preserve adequate molecular detail. Consideration of such models is rendered possible by computer simulation, given generous access to the high-performance computational machines that have become available recently. We have started a program of molecular dynamics simulation of passivated metal nanoparticles in supercritical fluids. Our aim is to elucidate, in terms of molecular interactions and structure, the key mechanisms underlying the dispersion of the nanoparticles in such fluids. Two inter-related aspects bearing strongly on the dispersion process are the solvation of the particles and the solvent-mediated interactions between them. The degree of solvation provides a good indication of the tendency of the particle to remain immersed in the solvent, and the particle−particle potential of mean force would determine whether the system is stable against aggregation. In this paper, the first on our current work, we present our simulation studies of the solvation of an 8-atom and a 38-atom gold nanoparticle in ethane in the subcritical−supercritical regime. We wish to explore the mode of the association of the solvent molecules with the

* Corresponding author. E-mail: mlal@liverpool.ac.uk.
† University of Liverpool.
‡ CCLRC Daresbury Laboratory.
§ Present address: Dept of Information Studies, University of Sheffield.

10.1021/jp036776e CCC: $27.50
Published on Web 04/17/2004

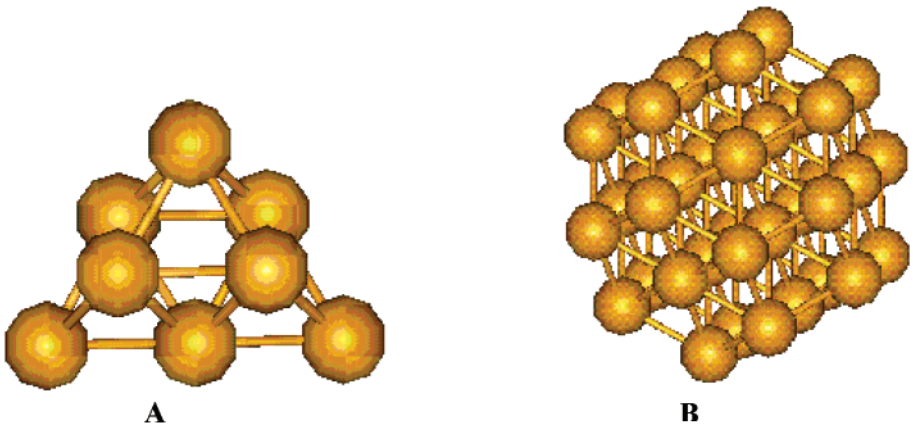

Figure 1. Initial structures of the 8-atom (A) and the 38-atom (B) cores.

particle and to see how the particle size would affect the degree of solvation. The simulations are performed along the critical isochore partly because of significant experimental interest in this phase region of the solvent in respect of extraction and separation processes and partly because it represents a direct pathway for the transition of the solvent from the subcritical to the supercritical regime through the critical point. The latter consideration will permit investigation of the temperature-dependent, special effects on the solvation process as the system approaches the critical point either from the subcritical or from the supercritical state.[33]

Although many simulation (MD and Monte Carlo) studies of bulk gold surfaces covered with terminally anchored alkane layers have been reported,[13,14] relatively few papers on ligand-covered particles have appeared in the literature. Luedtke and Landman performed MD simulations of 140-, 201- and 1289-atom gold particles passivated with $C_{12}H_{35}S$ ligands at saturation coverage.[15,16] Their work furnishes fascinating insights into the mode of assembly and configurational structure of the passivating layer of the isolated particle and the particle on the graphite surface. Further, through their simulations, they established the packing of the 140-atom particles into a bcc superlattice structure at 300 K, predicted to transform into an fcc structure at 350 K.[15] Hakkinen, Barnett, and Landman[17] reported DFT calculations on a 38-atom gold particle, passivated with 24 methyl thioate molecules, investigating its electronic structure, capacitance, energetics, and charging behavior. To our knowledge, few simulation studies of passivated nanoparticles immersed in a medium have been published heretofore.

2. Description of the Model

A. The Nanoparticles. A1. Metal-Atom Cores. The 8-atom gold cluster, constituting the core of one of the nanoparticles considered here, has been investigated theoretically by Rousseau and Marx[18] who performed Car−Parinello MD simulations on neutral and charged gold clusters of up to 15 atoms mainly to identify their low-energy configurational states and explore the nature of their interaction with methanol. The lowest-energy structure of the cluster yielded by their computation, shown in Figure 1A, has six atoms arranged in an octahedral morphology and the remaining two atoms located over two triangular faces of the octahedron, the structure possessing C_{2v} symmetry. The mean distance between nearest neighbors in the structure is 2.72 Å. As little experimental or other theoretical information is available on the interatomic configuration of this cluster, the structure emerging from the computation of Rousseau and Marx has been assumed as the initial configuration of the core of our particle.

The 38-atom Au cluster, the core of our second particle, has been predicted to assume face-centered cubic structure with a truncated octahedral morphology[7,19] (Figure 1B). Two regions may be distinguished in the cluster, an inner region of six atoms assuming an octahedral arrangement and an outer, surface region of 32 atoms possessing eight (111) and six (100) faces. The optimized structure of Cleveland et al.,[19] based on the embedded-atom potential,[20] served as the starting configuration for the core in the present simulations. In this structure the nearest-neighbor interatomic distances are equal to 2.82 Å in the inner region, 2.72 Å in the outer region, and 2.67 Å between the inner and the outer regions. Further DFT optimization of the cluster led to some narrowing of the nearest-neighbor distance range.

The interaction of the core atoms with the passivating layer and the solvent molecules is likely to change the initial configuration of the core to an extent, which has been allowed for in our simulations by permitting the structure to relax. The forces between gold atoms in the core derive from the many-body potentials whose generic form follows from two parallel formalisms, the embedded atom method (EAM) of Daw and Baskes[20] and the second-moment approximation to the tight binding theory of metals.[21] It consists of two terms, a pairwise additive term, and a many-body term:

$$U_{\text{core}} = \sum_{i<j} \phi_{ij} + F(\bar{\rho}) \tag{1}$$

where U_{core} is the interatomic potential energy of the core in a certain configuration. ϕ_{ij} is the pairwise additive contribution by the atom pair ij. $\bar{\rho}_i$, called the density term, is given by the linear superposition of the atomic densities around atom i. $\bar{\rho}_i = \sum_j \rho(r_{ij})$. F has a square-root dependence on $\bar{\rho}_i$, $F = -\epsilon C\bar{\rho}^{1/2}$, leading to

$$U_{\text{core}} = \sum_{i<j} \phi_{ij}(r_{ij}) - \epsilon C \sum_i \left(\sum_j \rho(r_{ij})\right)^{1/2} \tag{2}$$

Various functional forms for $\phi(r_{ij})$ and $\rho(r_{ij})$ have been proposed.[22] However, the inverse-power expressions render the potential to be in the familiar Lennard-Jones class with attendant advantage of ready scalability.

$$\phi(r_{ij}) = \epsilon\left(\frac{a}{r_{ij}}\right)^m, \quad \rho(r_{ij}) = \left(\frac{a}{r_{ij}}\right)^n \tag{3}$$

Sutton and Chen evaluated the parameters of this potential for various metals from their lattice and thermodynamic properties.[23] For gold, $C = 34.408$, $\epsilon = 1.234$ kJ/mol, $a = 4.08$ Å, $m = 10$, and $n = 8$, which are assumed in the present work.

TABLE 1

bond/bond angle/torsion	l_0 (Å)	k_b (kJ/mol Å^{-2})	θ_0 (deg)	k_θ (kJ/mol deg^{-2})	c_1 (kJ/mol)	c_2 (kJ/mol)	c_3 (kJ/mol)
CC	1.54	802.24					
CS	1.82	802.24					
CCC; CCS			114	0.158			
AuSC			104	0.058			
CCCC; SCCC					2.95	0.567	6.58

A2. Passivating Layer. In the present systems, the passivating layer surrounding the gold nanocore is formed by linear C_{12} alkane thioate molecules terminally linked to the core surface by the S−Au bond. The structural details of alkane molecules are known with a good degree of precision, which have served to build accurate atomistic models for these molecules for computer simulation studies.[24] However, recent studies published by several groups show convincingly that the united-atom models for these molecules, which are coarse-grained to the extent that the CH_2 and CH_3 groups in the chain are reduced to single interaction sites, are able to reproduce accurately the liquid-vapor coexistence curves. The interpolated values of the critical points obtained from these curves agree well with the experimental figures. The optimization process involved adjusting the values of various interaction parameters against the experimental liquid-vapor coexistence data of a given alkane system in Monte Carlo simulations and then subsequently establishing that the adjusted set of parameters are transferable to other alkanes in the computation of their coexistence curves. Three prominent sets of parameters optimized in this way are TraPPE, due to Siepmann and co-workers,[25] NERD, due to Nath et al.,[26] and the one due to Errington and Panagiotopoulos.[27] For our simulations we have selected the first, since it has a slight edge over the second in respect of reproducing the critical points and, compared to the third, it offers economy of parameters. It is perhaps worth stating that in the present work there is some merit in using the force fields that are consistent with experimental liquid vapor equilibria, since the phase region of interest is in the vicinity of the critical point.

The model for the passivating chains embodies the intramolecular geometry (bond lengths, bond angles, etc.), the potentials corresponding to bond stretching, bond angle bending and bond torsion, and the potentials for interactions between nonbonded atoms (united atoms in the present model).[24] The bond stretching, bond angle bending, and bond torsion energies are given by the potentials

$$U_b = {}^1/_2 k_b (l - l_0)^2 \tag{4a}$$

$$U_\theta = {}^1/_2 k_\theta (\theta - \theta_0)^2 \tag{4b}$$

$$U_\phi = c_1(1 + \cos\phi) - c_2(1 - \cos 2\phi) + c_3(1 + \cos 3\phi) \tag{4c}$$

where U_b, U_θ, and U_ϕ are, respectively, the bond stretching, bond bending and bond torsion energies. l_0 and θ_0 are the equilibrium values of the bond length and the bond angle. k_b and k_θ (the spring constants) are the potential parameters. ϕ is the torsion angle (i.e., the angle between the pair of planes formed by three successive bonds in the chain). c_1, c_2, and c_3 are the parameters of the torsion potential. Values of the various parameters featuring in the above potentials[24,25] are presented in Table 1

Nonbonded Interactions. The nonbonded interaction energy arises from the interactions between the atoms belonging to different chains, between those belonging to the same chain but separated by more than three bonds and between the chain atoms and the core atoms. Expressed in terms of the Lennard-Jones potential, these interactions are assumed to be pairwise additive.

TABLE 2

atom pair	ϵ (kJ/mol)	σ (Å)
CH_3/CH_3	0.8146	3.75
CH_2/CH_2	0.382	3.95
S/S	1.046[16]	4.45[16]
CH_3/CH_2	0.558	3.85
CH_3/S	0.923	4.10
CH_2/S	0.633	4.20
Au/CH_3, Au/CH_2	1.795[28]	4.45[28]

$$U_{ij} = 4\epsilon_{ij}[((\sigma_{ij}/r_{ij}))^{12} - ((\sigma_{ij}/r_{ij}))^6] \tag{5}$$

where U_{ij} is the interaction energy between a pair of nonbonded atoms a distance r_{ij} apart. The total nonbonded energy of the system in a given configuration is the sum of U_{ij} over all nonbonded pairs. ϵ_{ij} and σ_{ij} are the parameters characterizing the potential. Their values for the various pairs that feature in the present system are listed in Table 2, values for the unlike pairs calculated from the standard combining rules:[24] $\epsilon_{ij} = (\epsilon_{ii}.\epsilon_{jj})^{1/2}$; $\sigma_{ii} = (\sigma_{ii} + \sigma_{jj})/2$.

The Sulfur—Gold Bond. The interaction between S and Au atoms can be effectively represented by a Morse potential with the values of parameters adjusted against the relevant spectroscopic and thermodynamic properties:

$$U_M = U_0[\{1 - e_M^{-k}(r - r_0)\}^2 - 1] \tag{6}$$

where U_M is the interaction energy between the atom pair S/Au a distance r apart. There are two sets of the values of the parameters U_0, k_M, and r_0 published in the literature[16,29] with only minor numerical differences between them. Here we have selected the values quoted by Luetdke and Landman: $U_0 =$ 38.6 kJ/mol, $k_M = 1.3$ Å^{-1}, $r_0 = 2.9$ Å, obtained by them using experimental data on the binding energy and known values of the equilibrium distance and vibrational force constants of the S−Au bond.

B. The Solvent. The ethane molecule is modeled as a pair of covalently bonded united atoms representing the CH_3 groups. The parameters for characterizing the bonded and nonbonded interactions between the solvent methyls are assumed to be the same as for those belonging to the passivating chains, given in Tables 1 and 2 above.

3. Computational Details

The computations were performed using DL-POLY2, a parallel MD code developed by Daresbury Laboratory with leading participation by one of the authors.[30] The code has proved highly efficacious for simulating systems of complex, large polyatomic molecules[31] and is, therefore, eminently suitable for our purpose.

The passivated particle was immersed in a (100 Å × 100 Å × 100 Å) cubic cell containing the number of solvent molecules which corresponded with the critical density (ρ_c) of computer-simulated ethane (206 kg/m^3),[25] with the cell subjected to the usual periodic boundary conditions.

In generating the initial configuration, solvent molecules, in excess of the required number, were placed on a regular lattice with the nanoparticle at the center of the cell, the thioate chains attached to the core assuming the fully extended configurational states. Excess ethane molecules, particularly those too close to

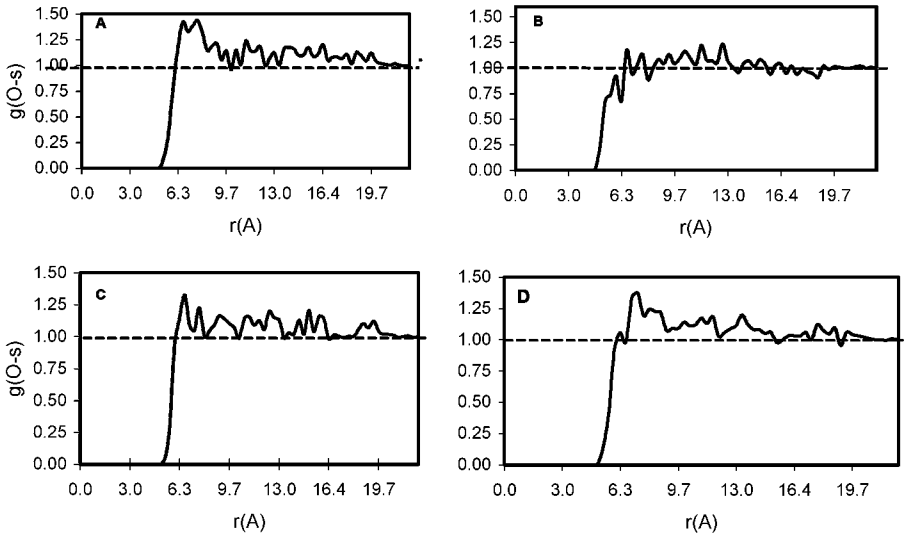

Figure 2. Radial distribution of the solvent interaction sites (i.e., methyl groups) about the core center of the 8-atom-core passivated particle at ρ_r ($=\rho/\rho_c$) equal to 1. Key: (A) T_r ($=T/T_c$) = 0.95; (B) T_r = 0.98; (C) T_r = 1.016; (D) T_r = 1.05. g(O−s) = 1 (bulk value).

the chains or the core, were removed from the cell to eliminate regions of high repulsive energy that might otherwise be detrimental to the stability of the system. All simulations were performed in the NVT ensemble (Hoover thermostat) with 1 fs time steps. Runs of 10^6 time steps were found sufficiently long for obtaining satisfactory convergences in the various properties of interest. The configurational data were saved at intervals of 100 steps in the post equilibration phase and used to analyze the system structure.

Two points in the present series of simulations lie in the liquid/vapor coexistence region, the subcritical regime. MD simulation studies of systems comprised of liquid/gas coexisting phases not far from the critical regime have been reported in the literature, notably by Tildesley and co-workers[36] and Honma et al.[37] These workers have successfully computed liquid/vapor coexistence densities leading to the estimation of ρ_c and T_c, in good agreement with experimental results. The simulation is rendered more difficult for the present system due to the fact that the points in question are located on the critical isochore close to the critical point, which would exacerbate the problems arising from heterogeneities and fluctuations in the density. In assessing the viability of performing successful MD simulations in our subcritical region, we carried out the simulation of pure ethane, which showed that the potential energy and the pressure converge satisfactorily at both points. Cluster analysis revealed that at T_r ($= T/T_c$) equal to 0.95 the molecules are populated in clusters with a bimodal size-distribution: there existed one (rarely two) very large, long-lived cluster with an abundance of small clusters. It was possible to compute the mean volume occupied by the large cluster, leading to an estimate of its mean density, 5.8 ± 0.5 molecules/nm^3, in reasonable agreement with the value of 6 molecules/nm^3 for the liquid density at this temperature, obtained by interpolating the Grand Canonical Ensemble Monte Carlo simulation data.[25] Thus, the large cluster observed in our simulation constitutes the liquid phase. At T_r = 0.98, our second point in the subcritical region, the cluster-size distribution lost its bimodal feature, so the distinction between the two phases was obliterated. At both points the application of the Hoover thermostat presented no serious problems. Demonstrating the capability of the DL-POLY code for simulating two-phase systems close to T_c, our simulations of pure ethane paved the way for studying the system of our present interest.

4. Results and Discussion

As our present purpose is to determine the temperature and core-size effects on the solvation of the nanoparticles, we have here focused mainly on the computation of the distribution of the solvent molecules around the core and of the degree of solvation. For the 8-atom-core particle, the MD runs were originally started with 10 passivating chains attached to it. Two of the chains were desorbed as the simulation progressed, which were eliminated from the system. The 8-chain passivated cluster showed no signs of dissociation in all simulation runs performed on the system. The 38-atom-core particle was passivated with 24 C_{12} thiolate chains with the initial positions of the sulfur atoms taken from the work of Cleveland et al.[17] The reduced temperature ($T_r = T/T_c$, where T_c is the critical temperature (304 K) of the simulated ethane[25]) range covered in our simulations of both systems is 0.95−1.05.

A. Radial Distribution of the Solvent Methyl Groups around the Core. The distribution was calculated simply by counting at intervals of 100 time steps and subsequently averaging over the equilibrated part of the sample, the number of the solvent methyl groups located between the radial distances ($r - \delta r$) and ($r + \delta r$) from the center of mass of the core, O, with δr equal to 0.1 Å, the calculation extended to a distance−typically 25 and 30 Å for the 8-atom-core and the 38-atom-core particles respectively−lying well outside the passivating layer at which the distribution would attain the bulk solvent limit. Figures 2 and 3 show typical distributions presented as g(O−s), equal to $\rho(r)/\rho$(bulk), as functions of r.

In the core region, g(O−s) is found to be zero, affirming the inaccessibility of the solvent molecules to the interior of the core. As r exceeds the core periphery, g(O−s) rises sharply, subsequently entering a regime which is conspicuous by the presence of oscillations. This regime corresponds with the outer, passivating layer of the particle. The distributions converge satisfactorily to the bulk behavior for r about 4 Å greater than the overall particle size (core size + layer thickness). We believe that the oscillations in the distribution functions are a consequence partly of the spatial interference caused by the chain segments of the passivating layer and partly of the system being in the vicinity of the critical point of the solvent where the equilibrium fluid structure is characterized by very significant inhomogenenities,[32] occasioned by either enhanced or dimin-

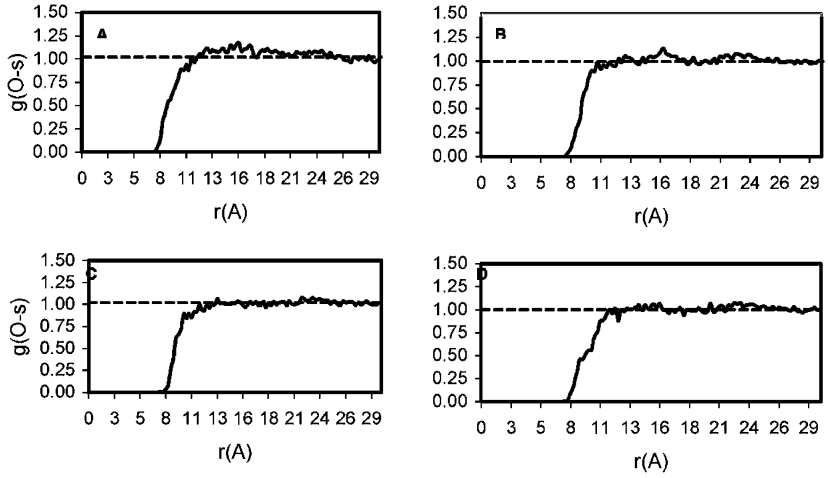

Figure 3. Radial distribution of the solvent interaction sites (i.e., methyl groups) about the core center of the 38-atom-core passivated particle at ρ_r ($=\rho/\rho_c$) equal to 1. Key: (A) T_r ($=T/T_c$) = 0.95; (B) T_r = 0.98; (C) T_r = 1.016; (D) T_r = 1.05.

ished clustering tendency of the molecules depending on the relative strengths of the like−like and unlike interactions in the system.

Superimposed on these effects is appreciable statistical noise which derives mainly from the fact that these distributions are computed about just one point, the center of mass of the core. Notwithstanding the noise, we have established that the distributions obtained from separate simulation runs with different initial configurations are closely similar, only minor variations occurring in the position and amplitude of the oscillations.

Although the distributions for both particles are qualitatively similar, there are significant quantitative differences which reside in the extent to which they depart from the bulk value (indicated by the dotted lines). In the case of the 8-atom-core particle, the departures are largely positive in the passivating-layer regime in the temperature range considered. At T_r = 0.95, the distribution possesses a distinct primary peak which is followed by an oscillatory regime lying above the g(O−s) = 1 line, the distribution converging to the bulk limit at $r \geq 20$ Å. As the system moves toward the critical point (T_r = 0.98), the primary peak is suppressed with the distribution lying partly above and partly below the g(O−s) = 1 line. In the supercritical regime (T_r = 1.016 and 1.05), the primary peak reemerges, with the positive departure being again predominant in the passivating-layer regime of the distribution. In the distributions for the 38-atom core particle, the primary peak feature is missing. Although in the subcritical regime (T_r equal to 0.95 and 0.98), there exist regions of measurable positive deviation, in the supercritical regime (C and D in Figure 3) much of the distribution lies quite close to the bulk line. Obviously, ± deviations of the distribution from the bulk value are of immediate consequence to the degree of solvation, to be discussed in the section to follow. It may be pointed out that the observed distributions are similar to those found by Petsche and Debenedetti for their repulsive systems close to the critical point.[33] For the passivated particles, the solvent distribution would be governed mainly by the solvent methyl/chain methylene interactions, which are somewhat weaker than the interactions between the solvent methyl/methyl groups, rendering the system to belong to the (weakly) repulsive class.

To ascertain how the presence of the passivating layer would modify the solvent distribution around the particle, we performed parallel simulations of a bare particle at the same temperatures and solvent density as assumed for the passivated particle simulations. The resulting distributions are presented in Figure 4.

In sharp contrast to the distributions corresponding to the passivated particle (Figure 3), the distribution of the solvent around the bare particle is dominated by a high primary peak. The peak height increases as the system moves toward the critical point and then decreases as it enters the supercritical regime. The distributions also feature a low-amplitude, secondary peak following which they converge to the bulk value with the level of noise characteristic of near-critical fluids. The high primary peak is indicative of strong adsorption of the solvent molecules at the particle surface. The mode of distribution suggests that the adsorbed layer consists of two regions, an inner high-density region corresponding with the primary peak and an outer lower density region corresponding with the secondary peak. The occurrence of the two peaks in the distribution also means that potential of the mean force between the particle and the solvent molecule has two minima, a deep primary minimum and a shallow secondary minimum. The positions of the minima—which would coincide with the positions of the peak maxima—are found, within the statistical error, to be insensitive to temperature variations in the range considered.

Since there are no passivating chains, the distribution of the solvent around the particle is governed by the balance between the Au/CH_3 and CH_3/CH_3 interactions. The ratio between the potential well depths, $\epsilon_{21}/\epsilon_{11}$, for the two pairs is 2.20. If the interactions of all nanoparticle gold atoms with the solvent methyl are added, the resulting potential would be much deeper, so the ratio in question could be as much as an order of magnitude higher than 2, which would entirely satisfy the necessary criterion ($\epsilon_{21}/\epsilon_{11} > 1$) to be applied in placing this system in the attractive class.[34] The simplest possible example of this class of systems is a xenon atom in near-critical neon, studied by Petsche and Debenedetti.[33] The $\epsilon_{21}/\epsilon_{11}$ ratio for that system is 7.04. It is noteworthy that the distribution of the neon atoms about Xe, obtained by these workers at ρ_r = 1 and T_r = 1.037, contains all the essential features exhibited by our distributions including the occurrence of a secondary peak.

B. The Degree of Solvation. The degree of solvation, ϑ, may be defined as the excess number of solvent molecules per core atom bound to the nanoparticle, which in terms of the particle−solvent distribution is expressible as

$$\vartheta = \frac{4\pi\rho_0}{N}\int_0^\infty [g(O-s) - 1]r^2\,dr \qquad (7)$$

where ρ_0 is the bulk density of the solvent and N is the number

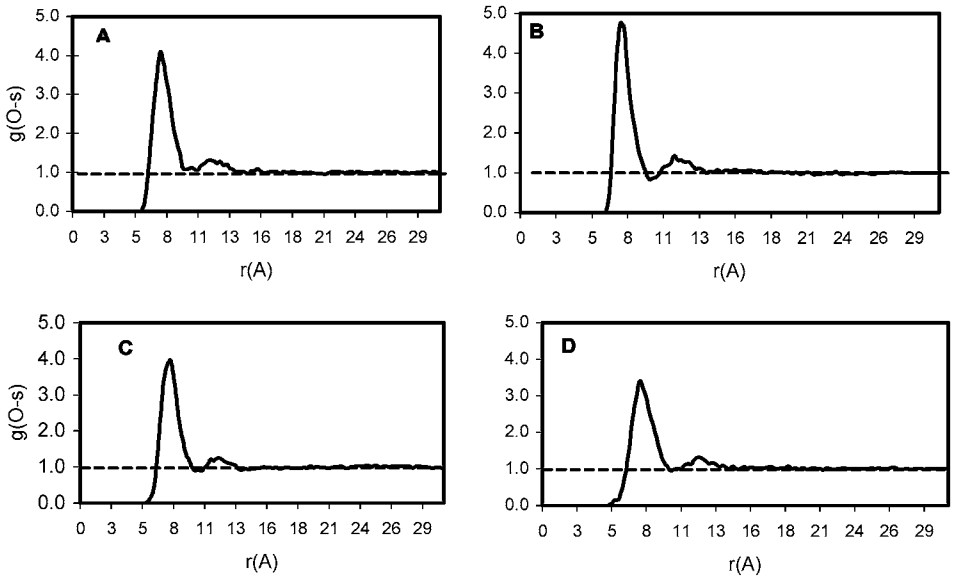

Figure 4. Radial distribution of the solvent interaction sites (*i.e.*, methyl groups) about the core center of the 38-atom-core bare particle at ρ_r (= ρ/ρ_c) equal to 1. Key: (A) T_r (=T/T_c) = 0.95; (B) T_r = 0.98; (C) T_r = 1.016; (D) T_r = 1.05. Dotted line: bulk value.

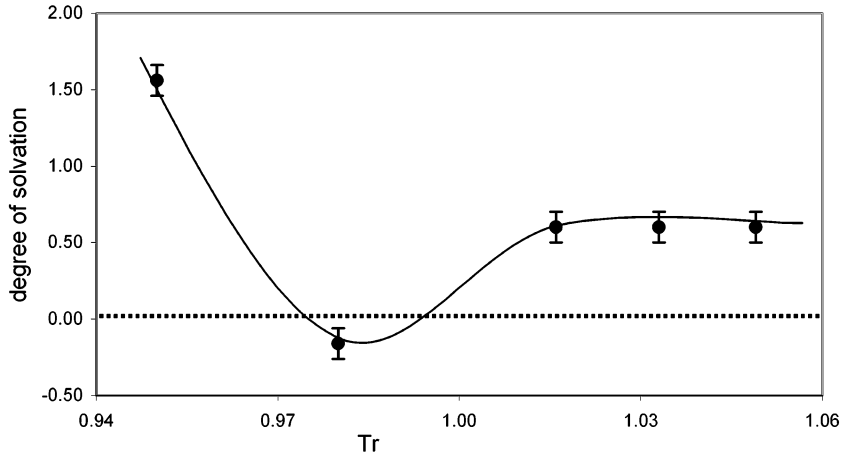

Figure 5. Degree of solvation (ϑ) vs reduced temperature ($T_r = T/T_c$) for the 8-atom-core passivated particle.

of atoms in the core. The integral on the rhs of the equation is known as the Kirkwood−Buff integral.[35] In the event of the availability of highly accurate numerical data on g(O−s), ϑ can be readily computed from eq 7. More simply, hence preferably, one may accumulate in a simulation run the data on the number of solvent molecules contained in a sphere with its center coincident with the center of mass of the core and its radius, R, equal to a distance that would be sufficiently large to ensure convergence of g(O−s) to 1. The difference between the mean number of solvent molecules in the enveloping sphere and $n_0 = {}^4/_3\pi R^3\rho_0$ will represent the excess number of solvent molecules bound to the particle. The values of R assumed for the 8-atom-core passivated particle, the 38-atom bare particle, and the 38-atom passivated particle were, respectively, 20 Å, 20, and 30 Å. The results for the three systems are displayed in Figures 5 and 6. The error bars shown in Figures were estimated by dividing the equilibrated part of the MD run (∼ 900 000 time steps) into 10 equal-sized sub-samples. "Local" value of ϑ for each sub-sample was obtained. The standard deviation of the local values from their mean was taken as the magnitude of error, represented by the bars. The standard deviation did not differ significantly from point to point. The lines joining the points are simply guides to the eye.

For the 8-atom-core passivated particle, ϑ is positive at T_r = 0.95, decreasing rapidly to a negative value as the temperature is increased to 0.98. In the supercritical regime ($T_r > 1$), ϑ reverts to positive values, which remain almost constant with increase in temperature. The degree of solvation for the 38-atom-core passivated particle, on the other hand, is mostly negative in the temperature range considered−it is only at the lowest temperature (T_r = 0.95) that it is slightly positive. This means that while for the smaller size nanoparticle ethane is a good solvent both in the subcritical and supercritical regimes, it is a poor solvent for the larger size particle. This finding is consistent with the experimentally observed trend in the size dependent dispersibility of passivated gold nanoparticles in supercritical ethane, although the experiments were performed on much larger particles.[10]

The contrasting characteristics of the solvent distributions in the bare and the passivated particles are also reflected in their degree of solvation, Figure 6. The degree of solvation for the bare particle is positive in the temperature range considered, whereas it is either nearly zero or negative for the passivated particle, a direct consequence of the former belonging to the attractive class of systems and the latter to the weakly repulsive class. In the former, the enhancement of the solvent concentration around the solute as the critical point is approached from either the subcritical or the supercritical regime is clearly evident in the ϑ results, presented in Figure 6A. Figure 6B shows that for our weakly repulsive system the depletion does occur as

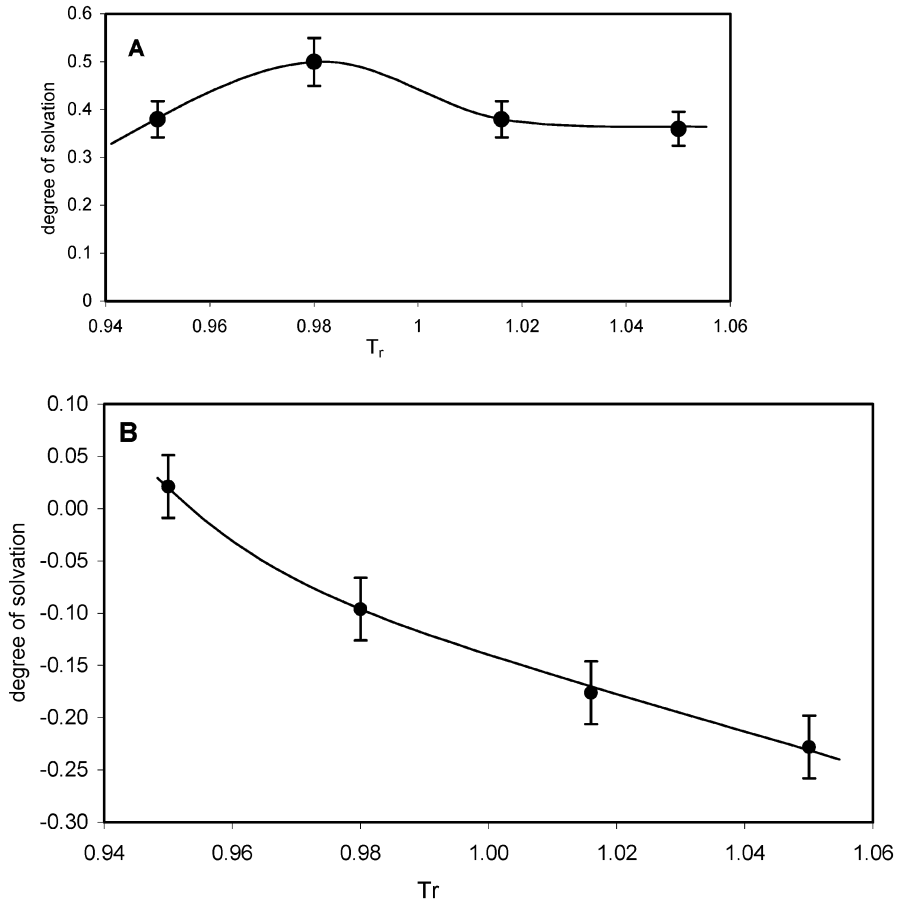

Figure 6. Degree of solvation vs reduced temperature for the 38-atom-core particle: (A) bare particle; (B) passivated particle.

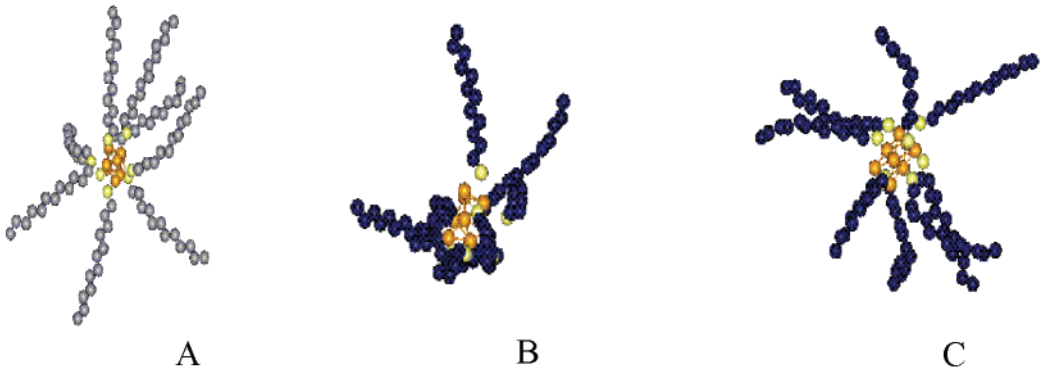

Figure 7. Illustrative snapshots of the 8-atom-core passivated particle taken from the equilibrated part of the simulation runs at different temperatures: (A) $T_r = 0.95$; (B) $T_r = 0.98$; (C) $T_r = 1.05$. For clarity, the solvents molecules have been omitted.

one approaches the critical point from the subcritical side but not from the supercritical side. Perhaps the ratio between the unlike and like-like interactions ($\epsilon_{21}/\epsilon_{11} = 0.68$) is not so small as to produce the effect in question.

The reason for the large difference found in the solvation capacity of the 8-atom-core and the 38-atom-core passivated particles lies essentially in the different structures of the passivating layers covering their core surfaces. In the case of the 8-atom core particle, the location of the anchoring sites allows the chains to extend out radially into the surrounding fluid providing an open structure for the passivating layer that would lend the solvent molecules easy access not only to the spaces between the chains but to the inner region, located in the immediate proximity of the core surface, where they would interact predominantly with the Au and S atoms. As the CH_3/Au and CH_3/S interactions are stronger than the CH_3/CH_2 and CH_3/CH_3 interactions, one would expect the solvent to occur in higher concentrations in the inner region. This is borne out by the occurrence of the pronounced primary peak in the distribution presented in Figure 2A.

At T_r equal to 0.95, the temperature corresponding to Figure 2A, the anchored chains are in an extended state (Figure 7A), indicated by their mean square end-to-end distance, $\langle L^2 \rangle$, equal to 235 Å^2. The increase in temperature permits increased number of gauche states to occur, leading to the collapse of a fraction of chains[39] ($\langle L^2 \rangle = 145$ Å^2 at $T_r = 0.98$), in turn destroying the open structure of the layer and so blocking access of the solvent molecules to the inner region. This is manifested in the distribution presented in Figure 2B, where we see that the pronounced peak found in Figure 2A has disappeared. The chain collapse is depicted by the snapshot presented in Figure 7B. At higher temperatures ($T_r > 1$), the anchored chains undergo

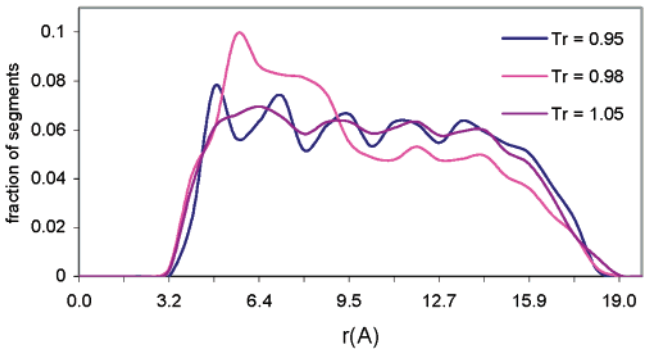

Figure 8. Distribution of chain segments in the passivating layer of the 8-atom-core particle, plotted as fraction of segments in successive shells of thickness $\delta r = 0.75$ Å as a function of r, the distance from the core center.

expansion (Figure 7C) allowing increased number of the solvent molecules to be accommodated in the layer. Thus, the 8-atom-core passivated particle in ethane represents an example of a hybrid system possessing both attractive and weakly repulsive types of behavior, the relative contribution of the two features to the degree of solvation depending on the temperature.

Salient features of the configurational structure of the passivating chains bearing on solvation may be discerned from the distribution of segments in the passivating layer, presented in Figures 8 and 10 for the 8-atom-core and the 38-atom-core particles, respectively.

The main factors governing the distribution include the confinement due to terminal anchoring, intramolecular geometry such as bond lengths and bond angles, bond torsion, and the nonbonded interactions (intrachain, chain/chain, core/chain and solvent/chain). Constant bond lengths and bond angles (the corresponding force fields permit only small variations in these quantities) would tend to regulate the spacing between the segments within the chain, in this way conferring some periodicity to the distribution. Bond torsion and the nonbonded interactions would perturb, substantially reduce or even eliminate the periodic behavior, depending on how dominant they are in the system.

The distribution corresponding to $T_r = 0.95$ for the 8-atom-core particle is characterized by distinct oscillations implying that the effects of bond torsion and nonbonded interactions are small, consonant with a configurational structure, where the chains are extended and well separated. The increase in the temperature to $T_r = 0.98$ results in a significant change in the distribution: a broad peak covering the distance range 4.5−9.5 Å appears, indicating the emergence of a region of appreciably higher segment concentration close to the core surface. The occurrence of this region is a clear evidence of the chain collapse at this temperature. The peak disappears at $T_r = 1.05$ as the collapsed chains expand.

Dictated by the configuration of the anchoring sites at the (111) face, the structure of the passivating layer covering the 38-atom core is close-packed. In the high-coverage limit (the present case), the chains belonging to the same anchoring face would tend to remain parallel to each other in a largely extended state, as revealed by the configurational states shown in Figure 9.

$\langle L^2 \rangle$ and the mean separation between the terminal methyl groups of the nearest-neighbor chains (i.e., the chains on the same anchoring face) were found to vary only slightly with temperature, indicating relatively low sensitivity of the layer structure to the temperature variations. Broad similarities found among the segment distributions shown in Figure 10 also lead to the same inference. The oscillatory character of the distributions, indicative of the prevalence of the extended state, is featured at all the temperatures. However, noticeable damping of the oscillations does occur as the temperature is increased, pointing to increasing influence of the nonbonded interactions and the bond torsion effects at higher temperatures.

In the close-pack limit, the inner region of the layer would be sterically shielded. Thus, most of the solvating molecules would be located in the outer region. This means, of course, that the solvation of this particle would be predominantly controlled by the weaker, chain/solvent interactions. The absence of the primary peaks in the distributions presented in Figure 3 substantiates the exclusion of the solvent molecules from the inner region of the passivating layer.

C. Structural Modification of the Core. It is instructive to see if the core undergoes significant structural changes that might be caused by its interactions with the passivating chains and /or with the solvent. In investigating these effects, we have, apart from collecting the position coordinates data for the core atoms in the simulations discussed above, performed additional simulations on both bare and passivated particles in the vacuum. The results showed that while in the vacuum the initial configuration of the bare core remains essentially unchanged in the temperature range studied, the configuration underwent appreciable changes for the passivated cores in the solvent, an effect of the external interactions imposed on the core by the presence of the chains, the solvent and, most importantly, the Au−S bond. These changes, identified from the variation of the metal-atom position coordinates with respect to the core center of mass as well as from the atom−atom radial distribution functions, occurred only in the preequilibration part of the simulation run, thereafter the core structure assuming a good degree of stability. The changes resulted in the deflation and loss of symmetry of the initial configuration (Figure 11), but were not so drastic as to cause core breakup or desorption of the passivating chains. These observations render untenable the assumption of invariant configuration for small cores, made in the studies of the particles of large core sizes.[15,16,38]

5. Concluding Remarks

A major conclusion of the present study is that in subcritical−supercritical ethane the solvation behaviors of the bare and the passivated metal nanoparticles are *qualitatively* different from each other. In the absence of the passivating layer, the degree and the mode of solvation is determined essentially by the metal-atom/solvent interactions, which are much stronger than the solvent/solvent interactions with the result that the degree of solvation of the bare particle is *positive* and large, a key feature of the *good* solvent condition. The presence of the passivating layer reduces the solvation capacity of the particle. The reduction can occur to such an extent as to render the degree of solvation *negativ*e, a characteristic of the *poor* solvent condition. The main reason for this lies in the passivating layer introducing two additional interactions bearing on the solvation process, the solvent/chain-segment and the solvent/S interactions, which are significantly weaker than the solvent/metal interactions.

The inducement of the enhancement effect by the proximity of the critical point is unequivocally shown by our results for the bare particle, the effect manifested in an increase of the height of the primary peak in the radial distribution of the solvent (Figure 4) as the system moves from the subcritical regime toward its critical point and a subsequent decrease in the peak height as it enters the supercritical regime. The occurrence of

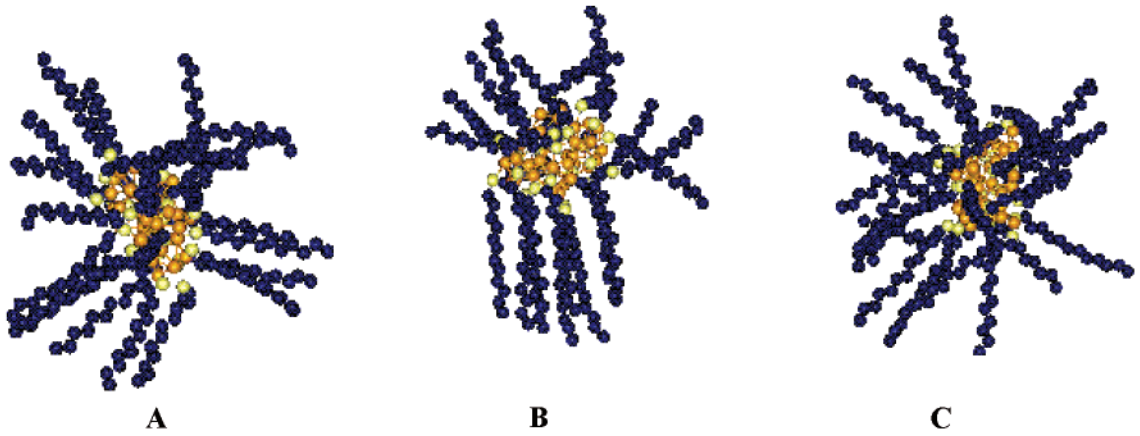

Figure 9. Illustrative snapshots, selected from equilibrated parts the MD runs, of the 38-atom core passivated particle depicting the configurational state of the passivating layer at $T_r = 0.95$ (A), $T_r = 0.98$ (B), and $T_r = 1.05$ (C). As in Figure 7, the solvent molecules have been omitted for clarity.

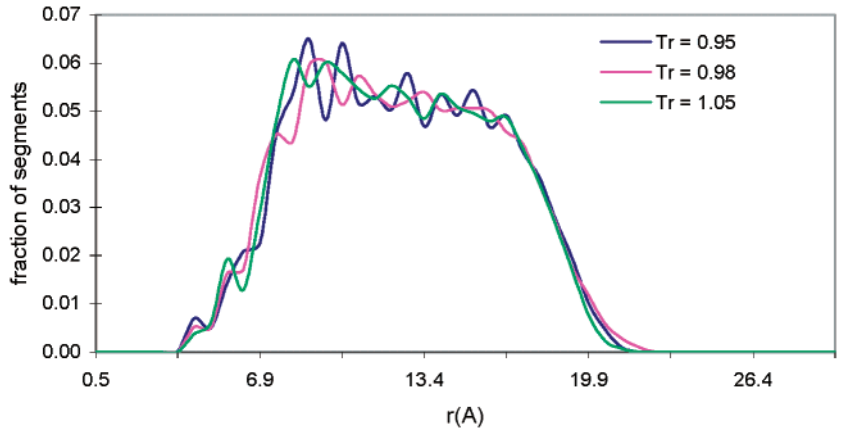

Figure 10. Chain segment distribution in the passivating layer of the 38-atom-core particle.

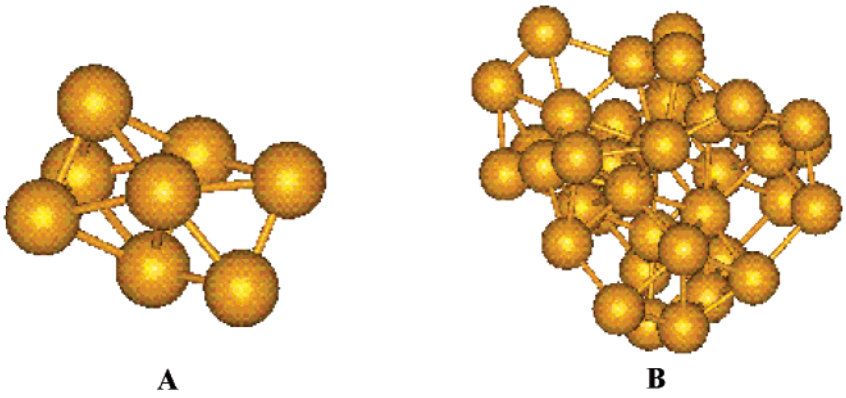

Figure 11. Equilibrium structures of the 8-atom and the 38-atom passivated cores at $T_r = 1.05$.

the maximum close to T_c in the ϑ vs T plot (Figure 6A) is also a consequence of the same effect. In the case of the 38-atom-core passivated particle—which falls in the category of weakly repulsive systems—our results do show the enhancement of depletion in the subcritical → critical direction but not in the supercritical → critical direction, i.e., no minimum in the ϑ vs T plot in Figure 6B. It is quite possible that in our system the difference in the solvent/solvent and the solvent/chain interactions is not sufficiently large to observe the enhancement effect in the solvent depletion around the particle. We believe that the minimum in the plot observed for the 8-atom-core passivated particle is due essentially to the configurational collapse of the passivating chains—coincidently close to the critical point of the solvent—and their subsequent expansion as the temperature is increased.

The configurational structure of the passivating layer has a significant effect both on the degree and the mode of solvation. The open structure, assumed by the layer on the 8-atom core, allows the solvent molecules to reach the core surface, the region of strong interaction. The tight packing of the chains on the 38-atom-core, on the other hands, would impose steric restrictions on the access of the solvent molecules to this region. Detailed analysis of the configurational properties of the chains as functions of the particle core size, surface coverage, solvent density, temperature and their length will be the subject of a separate publication.

The liquid/vapor biphasic nature of the subcritical regime poses several important questions which remain unresolved in the present study. For example, how are the two phases distributed in the passivating layer, and whether the particle is

preferentially located in the interfacial region or in one of the two phases. The first question can be addressed by performing detailed analysis of the position coordinates of the solvent molecules to establish the mode of solvent clustering, using a cluster analysis code able to cope with such complications as presented by the passivating chains. We shall turn to this issue following the development of an efficacious code for the purpose in question. The second question may be tackled by pursuing simulations with a cell divided into three sections, the middle section containing the liquid phase with the vapor phase present in the other two.[36,37] The probability distribution of the position of the center of mass of the particle across the cell would reveal its preferential location. Such simulations would be viable only if the system is not too close to the critical point. A further question is whether the radial distribution of the solvent about the center of mass of the particle would constitute an adequate representation of the mode of solvation. It is true that in heterogeneous systems radial distribution functions do not present a complete picture of the structure. However, here they do serve a useful purpose of allowing comparisons to be made of the solvent distribution around the particle core in the subcritical and supercritical regimes.

In addition to dealing with the foregoing issues, our future work will extend to larger-size particles, focusing on the effects of solvent density, length of the passivating chains and the surface coverage on their solvation properties in the supercritical regime. In addition, simulations will be directed to the computation of potential of the mean force between the particles in a range of thermodynamic conditions corresponding to this regime.

Acknowledgment. Acknowledgments are due to Unilever Research for the award of a Research Fellowship to N.J.R. and to Computational Materials Chemistry Consortium of EPSRC (U.K.) for generous allocation of computational and manpower resources which made this work possible.

References and Notes

(1) Feldheim, D. L.; Foss, C. A. *Metal Nanoparticles: Synthesis, Characterization and Applications*; Marcel Dekker: New York, 2001.

(2) Zhang, J. Z.; Wang, Z.-L.; Lu, J.; Chen, S.; Liu, G.-Y *Self-Assembled Nanostructures*; Kluwer Academic/Plenum Publisher: New York, 2003.

(3) Alivisatos, A. P. *J. Phys. Chem.* **1996**, *100*, 13226.

(4) Rao, C. N. R.; Kulkarni, G. U.; Govindaraj, A.; Satishkumar, B. C.; Thomas, P. J. *Pure Appl. Chem.* **2000**, *72*, 21.

(5) Kelly, K. L.; Coronado, E.; Zhao, L. L.; Schatz, G. C. *J. Phys. Chem.* **2003**, *107*, 668.

(6) Schaaff, T. G.; Shafigullin, M. N.; Khoury, J. T.; Vezmar, I.; Whetten, R. L.; Cullen, W. G.; First, P. N.; Gutierrez-Wing, C.; Ascensio, J.; Jose-Yacaman, M. J. *J. Phys. Chem. B* **1997**, *101*, 7883.

(7) Cleveland, C. L.; Landman, U.; Schaaff, T. G.; Shafigulin, M. N.; Stephens, P. W.; Whetten, R. L. *Phys. Rev. Lett.* **1997**, *79*, 1873.

(8) Whetten, R. L.; Khoury, J. T.; Alvarez, M. M.; Murthy, S.; Vesmar, I.; Wang, Z. L.; Stephens, P. W.; Cleveland, C. L.; Luedtke, W. D.; Landman, U. *Adv. Mater.* **1996**, *8*, 428.

(9) Shah, P. S.; Holmes, J. D.; Doty, R. C.; Johnston, K. P.; Korgel, B. A. *J. Am. Chem. Soc.* **2000**, *122*, 4245. Korgel, B. A.; Fullam, S.; Connolly, S.; Fitzmaurice, D. *J. Phys. Chem. B* **1998**, *102*, 8379.

(10) Clark, N. Z.; Waters, C.; Johnson, K. A.; Satherley, J.; Schiffrin, D. J. *Langmuir* **2001**, *17*, 6048.

(11) Shah, P. S.; Holmes, J. D.; Johnston, K. P.; Korgel, B. A. *J. Phys. Chem. B* **2002**, *106*, 2545.

(12) Hunter, R. J. *Foundations of Colloid Science*; Oxford University Press: Oxford, U.K., 2000.

(13) Fischer, D.; Curioni, A.; Andreoni, W. *Langmuir* **2003**, *19*, 3567. Li, B.; Zeng, C.; Li, Q.; Wang, B.; Yuan, L.; Wang, H.; Yang, J.; Hou, J. G.; Zhu, Q. *J. Phys. Chem. B* **2003**, *107*, 972. Zhang, L.; Goddard, W. A., III; Jiang, S. *J. Chem. Phys.* **2002**, *117*, 7342. Shevade, A. V.; Zhou, J.; Zin, M. T.; Jiang, S. *Langmuir* **2001**, *17*, 7566. Sieval, A. B.; van den Hout, B.; Zuilhof, H.; Sudholter, E. J. R. *Langmuir* **2001**, *17*, 2172. Li, T.-W.; Chao, I.; Tao, Y.-T *J. Phys. Chem.* **1998**, *102*, 2935. Mar, W.; Klein, M. L. *Langmuir* **1994**, *10*, 188.

(14) Bhatia, R.; Garrison, B. J. *Langmuir* **1997**, *13*, 4038.

(15) Luedtke, W. D.; Landman, U. *J. Phys. Chem.* **1996**, *100*, 13323.

(16) Luedtke, W. D.; Landman, U. *J. Phys. Chem.* **1998**, *102*, 6566.

(17) Hakkinen, H.; Barnett, R. N.; Landman, U. *Phys. Rev. Lett.* **1999**, *82*, 3264.

(18) Rousseau, R.; Marx, D. *J. Chem. Phys.* **2001**, *112*, 761.

(19) Cleveland, C. L.; Landman, U.; Shafigullin, M. N.; Stephens, P. W.; Whetten, R. L. *Z. Phys. D* **1997**, *40*, 503.

(20) Daw, M. S.; Baskes, M. I. *Phys. Rev. Lett.* **1983**, *50*, 1285; *Phys. Rev B* **1984**, *29*, 6443.

(21) Finnis, M. W.; Sinclair, J. E. *Philos. Mag. A* **1984**, *50*, 45; **1986**, *53*, 161.

(22) Voter, A. F. In *Intermetallic Compunds, Vol. 1: Principles*; Westbrook, J. H., Fleischer, R. L., Eds.; John Wiley: New York, 1994; pp 77−90.

(23) Sutton, A. P.; Chen, J. *Philos. Mag. Lett.* **1990**, *61*, 139.

(24) Leach, A. R. *Molecular Modelling: Principles and Applications*; Prentice Hall/Pearson Education: London, 2001.

(25) Matin, M. G.; Siepmann, J. I. *J. Phys. Chem. B* **1998**, *102*, 2569. Wick, C. D.; Martin, M. G.; Siepmann, J. I. *J. Phys. Chem. B* **2000**, *104*, 8008. Wick, C. D.; Siepmann, J. I.; Schure, M. R. *J. Phys. Chem. B* **2001**, *105*, 10961.

(26) Nath, S. K.; Escobedo, F. A.; de Pablo, J. J. *J. Chem. Phys.* **1998**, *108*, 9905.

(27) Errington, J. R.; Panagiotopoulos, A. Z. *J. Phys. Chem. B* **1999**, *103*, 6322.

(28) Xia, T. K.; Ouyang, J.; Ribarsky, M. W.; Landman, U. *Phys. Rev. Lett.* **1992**, *69*, 1967.

(29) Mahaffy, R.; Bhatia, R.; Garrison, B. J. *J. Phys. Chem. B* **1997**, *101*, 771.

(30) Smith, W.; Forestor, T. R. *DL_POLY Package for Molecular Dynamics Simulations*; Daresbury Laboratory: Daresbury, U.K., 1999.

(31) Smith, W.; Yong, C. W.; Rodger, P. M. *Mol. Simul.* **2002**, *28*, 385.

(32) Martinez, H. L.; Ravi, R.; Tucker, S. C. *J. Chem. Phys.* **1996**, *104*, 1067.

(33) Petsche, I. B.; Debenedetti, P. G. *J. Chem. Phys.* **1989**, *91*, 7075.

(34) Debenedetti, P. G.; Mohamed, R. S. *J. Chem. Phys.* **1989**, *90*, 4528.

(35) Ben-Naim, A. *J. Chem. Phys.* **1977**, *67*, 4884; **1989**, *93*, 3809; *Pure Appl. Chem.* **1990**, *62*, 25.

(36) Alejandre, J.; Tildesley, D. J.; Chapela, G. A. *J. Chem. Phys.* **1995**, *102*, 4574.

(37) Honma, T.; Liew, C. C.; Inomata, H.; Arai, K. *J. Phys. Chem. A* **2003**, *107*, 3960.

(38) Powell, C.; Fenwick, N.; Bresme, F.; Quirke, N. *Colloids Surf.* **2001**, *206*, 241.

(39) Collapse of all the chains at the same time appears to be precluded by the excluded volume constraint in the region close to the core surface.